ACS OMEGA

Open Access

http://pubs.acs.org/journal/acsodf

Article

Single-Probe Sensing Array Based on Au Nanozyme for Simple, Rapid, and Low-Cost Colorimetric Identification of Antioxidants

Yu Wang, Yumeng Liu, Lidong Cao, Zunqiang Xiao, Yi Lu,* and Xin Zhang*

Cite This: *ACS Omega* 2025, 10, 6359−6367

Read Online

ACCESS | Metrics & More | Article Recommendations | Supporting Information

ABSTRACT: Identification of biological antioxidants is of vital importance because of the essential role of antioxidants in keeping the balance of various diseases. Here, we designed a simple, rapid, and low-cost nanozyme sensing array for colorimetric identification of multiple antioxidants based on Au nanoparticles (Au NPs) synthesized via a facile and green aqueous phase method. In the presence of H_2O_2, Au NPs possessed peroxidase-like catalytic activity and could effectively catalyze the color-less 3,3′,5,5′-tetramethylbenzidine (TMB) to blue oxidized product with comparable enzyme kinetics parameters. The function of the colorimetric sensing array was based on the inhibitory effect of diverse antioxidants on the chromogenic system to varying degrees under different pH conditions, resulting in various "turn-off" colorimetric signal responses. Based on the developed sensing array, four kinds of antioxidants with various concentrations and different proportions of the mixtures were successfully discriminated from each other with the aid of principal component analysis. Moreover, the sensing array showed good performance in differentiating antioxidants in human serum samples, which broaden the analytical application of Au NPs. Compared with the existing sensing array, the single Au NP-based sensing array significantly simplified the sensing element and detection process, opening a new avenue for biological molecule identification in real complex samples.

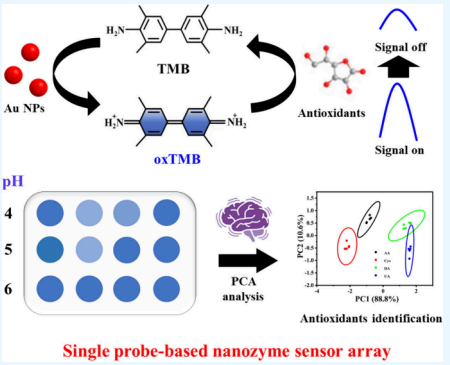

1. INTRODUCTION

Antioxidants are a class of biomolecules that prevent or slow down free radical formation in the body to reduce cellular damage and oxidative stress.[1] Antioxidants in biological fluids have been reported to play a significant role in the treatment and prevention of diverse diseases such as aging prevention, cancer, cardiovascular disease, and Alzheimer's disease.[2−4] Since antioxidants play important roles in a wide range of biological processes and diseases, there is an urgent need for effective and sensitive antioxidant assays in clinical practice. Currently, many analytical methods have been reported for antioxidant levels detection, such as conventional high-performance liquid chromatography (HPLC),[5] gas chromatography,[6] electrochemical sensors,[7] and fluorescence methods.[8] Although these approaches can be effective in the detection of antioxidants, they inevitably have corresponding limitations including expensive testing equipment, high requirements for operational expertise, high testing costs, and time-consuming sample processing.

In recent years, researchers have developed a lot of colorimetric sensors for the individual antioxidant detection due to the important advantages of the colorimetry, such as low cost, high sensitivity, good reproducibility, simple experimental operation, and ease of visual read-out.[9−11] However, it is impossible for a single antioxidant component to exist in a living system. Various antioxidant components either coexist or react with each other in a complex manner.[12] Therefore, colorimetric sensing arrays consist of multiple sensing units break through the limitations of the specific "lock-and-key" identification mechanism of conventional detection methods.[13] Depending on the characteristics of different targets, the colorimetric sensing arrays can generate cross-reactive signals, allowing simultaneous recognition of various targets without selectivity problems.[14]

Nanozymes are nanomaterials with natural enzyme-like catalytic effects, capable of catalyzing the reaction between substrates and enzymes under physiological conditions.[15,16] Compared to natural enzymes, nanozymes show many advantages such as low preparation cost, a simple preparation method, improved stability, and adjustable catalytic performance, which make them good alternatives for constructing colorimetric methods for the bioanalysis of diverse substances.[17−19] Since the Fe_3O_4 nanozymes with peroxidase (POD) properties were reported in 2007,[20] various nanozymes with enzyme-catalyzed properties have been investigated, such as Au,[21] Pt,[22] Co_3O_4,[23] MnO_2,[24] and MoS_2.[25] To date, several

Received: April 10, 2024
Revised: December 13, 2024
Accepted: January 28, 2025
Published: February 10, 2025

nanozyme-based colorimetric sensing arrays have been designed for the identification and detection of antioxidants in biological samples. For instance, Chen et al. designed a sensing array for colorimetric identification of antioxidants based on the catalysis of classical H_2O_2-3,3′,5,5′-tetramethylbenzidine (TMB) chromogenic system by various nanozymes including graphene oxide, MoS_2 and WS_2.[26] The presence of different antioxidants inhibited the chromogenic system to varying degrees, and the colorimetric response signals were utilized for the quantification and identification of these low concentrations of antioxidants in serum samples after pattern recognition methods. Li et al. reported a sensing array for antioxidants identification based on the oxidase-like activity of Fe−N/C single-atom nanozyme that can catalyze the oxidation of three chromogenic substrates including TMB, 2,2′-azinobis-(3-ethylbenzthiazoline-6-sulfonate) (ABTS), and 1,2-diaminobenzene (OPD).[27] The diverse chromogenic substrate-based sensing array can not only quantitatively detect individual antioxidants but also distinguish binary or ternary mixtures in human serum samples. Although these methods have been successfully used for the antioxidant identification and detection in biological samples, they are relatively complex, as they require a variety of nanozyme materials or chromogenic substrates to construct the sensing arrays. Simplification of the sensing array components is of great value for their further practical application.

With excellent optical and electrical properties, gold nanoparticles (Au NPs) can be used as signal recognition elements or readout probes and have been widely used in biochemical analysis.[28] For instance, optical fiber-based biosensors have been shown to enable detection of biomolecules in a faster, smaller and simpler way.[29] Marques et al. constructed a series of optical fiber-based biosensors using the local surface plasmon resonance (LSPR) effect of Au NPs.[30,31] They found that the sensitivity of the biosensors was also related to the fiber structure. The WaveFlex fiber structure provides a larger functionalized surface area, promotes the leakage of electrical waves from the core into the surrounding medium, and effectively enhances the LSPR effect of Au NPs.[30] Hence, the Au NPs coating significantly improves the sensitivity of optical fiber-based biosensors compared with bare fibers. Typically, Au NPs can be simply prepared by classical sodium citrate reduction method for diverse applications.[32−34] However, colorimetric sensing arrays based on their nanozyme activity of Au NPs have been less reported.

Here, we developed a colorimetric sensing array based on single probe materials (Au NPs) and single chromogenic substrates (TMB) for antioxidant identification and detection (Figure 1). First, Au NPs with a uniform spherical shape were synthesized using sodium citrate reduction. It was found that the Au NPs exhibited POD-like catalytic properties and the nanozyme activity varied at different pH. Accordingly, the construction of the colorimetric arrays was achieved by varying the different pH values of the chromogenic solution. Specifically, the reaction between H_2O_2 and TMB was significantly catalyzed by Au NPs at three pH values (pH 4, 5 and 6), producing different amounts of oxidized TMB (oxTMB) with obvious blue color. When antioxidants are present, oxTMB is reduced to varying degrees, resulting in a discoloration of the system and producing a "turn-off" colorimetric signal response. When combined with principal component analysis (PCA), this single-probe array successfully achieved simultaneous detection of four common representative antioxidants of serum and biological samples, such as dopamine (DA), ascorbic acid (AA), uric acid (UA), and L-cysteine (Cys).[35,36] Besides, the developed sensing arrays successfully identify different antioxidants at various concentrations and antioxidant mixtures at certain ratios. In practical tests, the array successfully differentiated serum samples spiked with different antioxidants, demonstrating the potential application of this sensing array in clinical diagnosis.

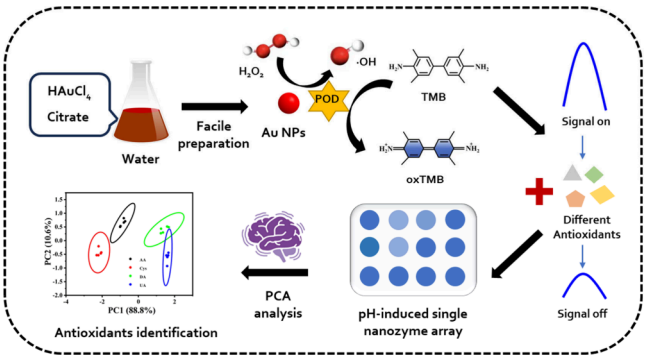

Figure 1. Schematic illustration for the facile preparation of the Au NPs with POD catalytic activity and their further application for antioxidant identification based on a pH-induced single nanozyme array and PCA analysis.

2. EXPERIMENTAL METHODS

2.1. Chemicals. All reagents were analytical grade and used without further purification. ascorbic acid (AA), 3,3′,5,5′-tetramethylbenzidine dihydrochloride (TMB), glucose (Glu), cholesterol (Cho), sodium chloride (NaCl), L-cysteine (Cys), and dopamine (DA) were commercially purchased from Macklin (Shanghai, China). Dimethyl sulfoxide (DMSO), H_2O_2 (30 wt %), bovine serum albumin (BSA), hydrochloric acid (HCl) and citrate were obtained from Sinopharm Chemical Reagent Co., Ltd. (Shanghai, China). Thiazole blue (MTT) Calcein-AM agent was obtained from Aladdin Reagent Co., Ltd. Hela cells were obtained from the Center for Typical Culture Collection. Human serum was purchased from Aldrich. All of the solutions in this work were prepared using ultrapure water (18.2 MΩ cm).

2.2. Preparation of Au NPs. The Au NPs were prepared according to the following procedure: 73 μL of $HAuCl_4$ (29 mM) solution was added to 1000 μL of deionized water, followed by addition of 150 μL of citrate (10 mg/mL) solution. Then, the above mixture was incubated for 1 h at 100 °C. The Au NPs were obtained after dialysis.

2.3. Characterization Apparatus. The UV−vis absorbance was recorded by using a UV-2450 spectrometer (Shimadzu). The morphology of the Au NPs were observed by transmission electron microscope (HT 7700). The zeta potential and hydrodynamic particle size of the nanoparticles were obtained by using a laser particle size meter (Zetasizer Nano-ZS90). The electron paramagnetic resonance (EPR) spectra was recorded on an EMX-10/12 spectrometer (Bruker, Germany). The cytocompatibility was measured with a multifunction microplate reader (SpectraMax M2). The fluorescent images of Hela cells were captured on an inverted fluorescence microscope (Olympus IX53, Japan).

2.4. Nanozyme Activity Test. The nanozyme effect of Au NPs was tested by virtue of the TMB oxidation in the presence of H_2O_2 using a UV spectrometer. Specifically, POD-like

https://doi.org/10.1021/acsomega.4c03460
ACS Omega 2025, 10, 6359−6367

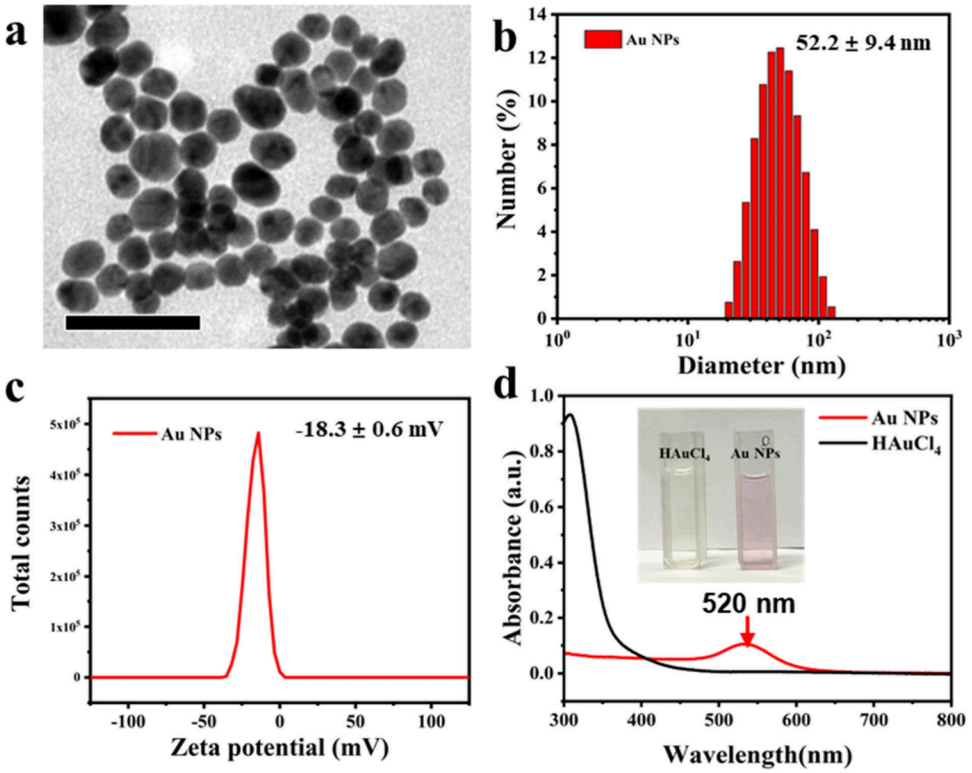

Figure 2. (a) Representative TEM images of prepared Au NPs. The scale bar is 200 nm. (b) The corresponding particle size statistics of prepared Au NPs by DLS. (c) The corresponding zeta potential statistics of prepared Au NPs. (d) UV−vis absorption spectra and the typical photos of different Au substances including $HAuCl_4$ and prepared Au NPs.

activity was determined according to the following procedure. First, 200 μL Au NPs was added to a 2 mL centrifuge tube. Following this, 300 μL of H_2O_2 solution (0.2 M) and 1000 μL of NaAc-HAc buffer solution (0.2 M) containing 0.6 mM TMB were added. The mixed solution was then incubated for 5 min at room temperature. Finally, the absorbance was determined by UV−vis spectrometer. To study the catalytic kinetics, the time-dependent absorbance at 652 nm was then tested using a UV−vis spectrometer. The amount of buffer solution was 1000 μL, containing different amounts of H_2O_2. The kinetics parameter including Michaelis−Menten constant (K_m) and maximum reaction rate (V_{max}) were calculated according to the double reciprocal curve of the Michaelis−Menten equation:

$$\frac{1}{V} = \left(\frac{K_m}{V_{max}}\right)\left(\frac{1}{[S]}\right) + \frac{1}{V_{max}}$$

where V stands for the initial velocity, K_m stands for the Michaelis constant, V_{max} means the maximum reaction rate, and S means the substrate concentration.

To find the best temperature, 200 μL of Au NPs was added to a centrifuge tube containing 300 μL of NaAc-HAc buffer solution at different temperatures (25−50 °C). To find the best pH, 200 μL of Au NPs was added to a centrifuge tube containing 300 μL of NaAc-HAc buffer solution with different pH levels (2−8). Three control groups were assigned at the same time.

2.6. Detection and Identification of Antioxidants. The antioxidant detection and recognition were conducted as follows: First, 200 μL Au NPs was added to a 2 mL centrifuge tube. Following this, 300 μL H_2O_2 solution (0.2 M) were added to 1000 μL NaAc-HAc buffer solution containing 0.6 mM TMB at different pH, followed by the addition of 200 μL different antioxidant (DA, AA, Cys, UA). After reaction for 15 min at 40 °C, the absorbance change (ΔA) at 652 nm of the sensing systems was measured and calculated. This process for four kinds of antioxidants was repeated 5 times. Then, the signals obtained from the sensing array were analyzed by principal component analysis (PCA) and hierarchical cluster analysis (HCA) on the original data matrix, using Origin 2021 software.

3. RESULTS AND DISCUSSION

3.1. Synthesis and Characterization of Au NPs. In this work, we used a facile and green aqueous phase synthesis method to prepare Au NPs as sensing probe.[32] During the process, sodium citrate was utilized as both a stabilizing and reducing agent for the chemical synthesis of Au NPs from $HAuCl_4$. It is worth noting that the chemical reduction method for Au NPs synthesis is very convenient and simple and thus beneficial for the further practical application of sensors. The morphology of prepared Au NPs was first characterized by transmission electron microscope (TEM). Figure 2a showed that the Au NPs were spherical in shape with relatively homogeneous distribution, indicating the successful preparation of Au NPs. Next, the hydrodynamic sizes and zeta potentials of Au NPs are characterized by dynamic light scattering (DLS). As indicated in Figure 2b, the resulting Au NPs exhibited an average size of 52.2 nm. As indicated in Figure 2c, the zeta potential of Au NPs was −18.3 ± 0.6 mV, demonstrating their good stability and dispersion in aqueous solution. Compared to $HAuCl_4$, the red color and characteristic absorption of Au NPs with an obvious absorption band at

https://doi.org/10.1021/acsomega.4c03460
ACS Omega 2025, 10, 6359−6367

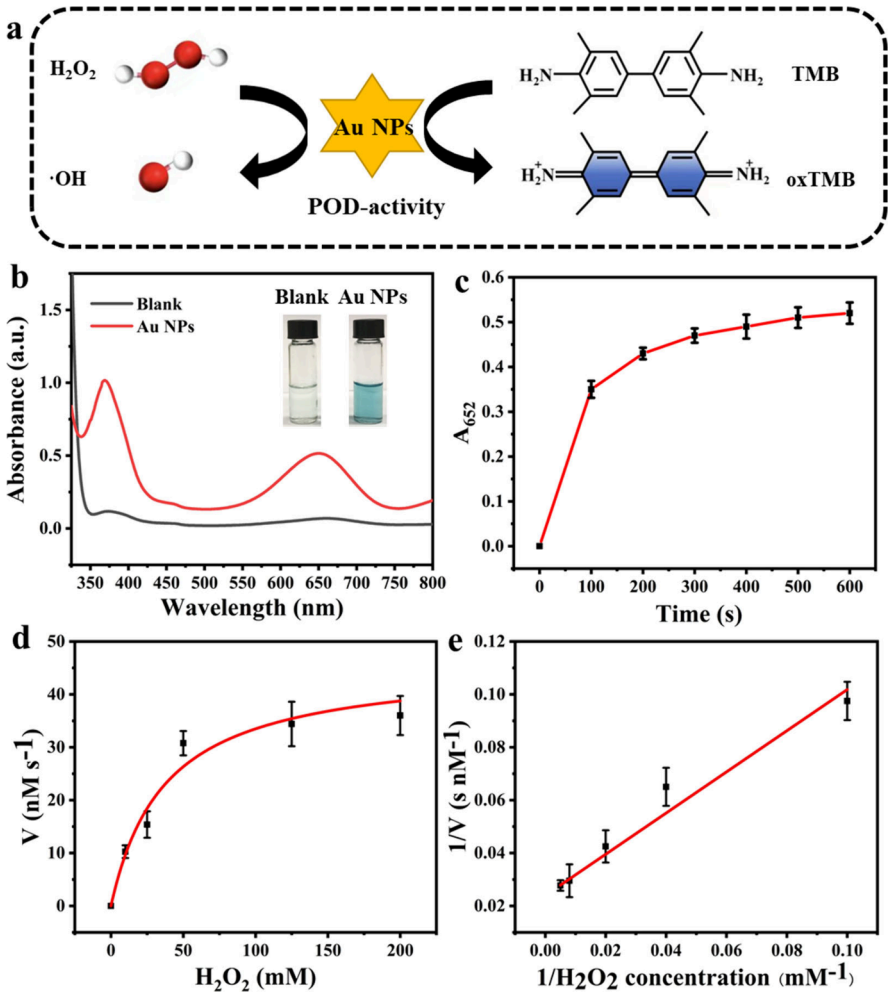

Figure 3. (a) Schematic for reaction process of H_2O_2 + TMB system catalyzed using the Au NPs. (b) The UV−vis absorption spectra and the corresponding photos of different reaction solutions after reaction for 10 min. (Blank, TMB + H_2O_2; Au NPs, TMB + H_2O_2 + Au NPs). (c) Time-dependent curves of absorbance at 652 nm of TMB + H_2O_2 + Au NPs solutions for 10 min. Steady-state kinetic test of Au NPs toward H_2O_2 including kinetic curve (d) and corresponding double reciprocal curve (e).

520 nm further suggested the formation of Au NPs (Figure 2d).

3.2. Nanozyme Catalytic Effect of Au NPs. TMB is one of the most commonly used POD chromogenic substrates. Here, we investigated the POD-like catalytic effect of Au NPs by using the classical H_2O_2-TMB system. As shown in Figure 3a, Au NPs with POD activity can effectively catalyze the decomposition of H_2O_2 into two hydroxyl radicals (·OH), which can further catalyze the TMB oxidation and produce the blue oxTMB product. As demonstrated in Figure 3b, the absorption peaks were not observed for the H_2O_2-TMB mixture. When Au NPs, H_2O_2, and TMB coexisted, the reaction system changed from colorless to obvious blue, and an apparent UV−vis absorption peak appeared at 652 nm. The above results indicated that the prepared Au NPs could catalyze the oxidation reaction of TMB by H_2O_2 with a POD-like activity. As indicated in Figure 3c, the absorbance of the reaction system at 652 nm increased with the increase of reaction time, and the reaction could reach equilibrium in about 5 min, which indicated the fast speed of the color development system. Many metal nanozymes have oxidase-like activity, which can be validated by testing the change in oxTMB absorbance without the addition of H_2O_2.[37] As shown in Figure S1, the direct reaction of nanozymes with TMB could not produce a signal at 652 nm within 30 min. Therefore, Au nanozyme lacks oxidase-like activity, and the color-development signal of the system originates from its POD-like activity.

Subsequently, the steady-state kinetics of the catalytic oxidation of TMB by Au NPs were analyzed by detecting the absorption value at 652 nm. As depicted in Figure 3d, the reaction of the H_2O_2 oxidation of TMB catalyzed by Au NPs followed the typical Michaelis−Menten kinetic model over the examined range of H_2O_2 concentrations. The curves fitted by the Lineweaver−Burk double inverse relationship are shown in Figure 3e, indicating that $1/V$ is linearly correlated with $1/S$. The apparent kinetic parameters of the catalytic reaction including Michaelis−Menten constant (K_m) and the maximum reaction rate (V_{max}) can be calculated from the slope and the intercept as 36.5 mM and 47.9×10^{-8} nM s^{-1}, respectively. K_m is the substrate concentration when the reaction rate is $1/2V_{max}$, which reflects the affinity of the enzyme for the H_2O_2 substrate. The smaller K_m value represents the stronger nanozyme affinity for the H_2O_2 substrate. As listed in Table 1, Au NPs possess smaller K_m values for H_2O_2 in comparison with Fe_3O_4 nanozyme, indicating the higher affinity of Au NPs. Compared to other Au-based nanozymes or HRP, Au NPs show the higher V_{max} values, demonstrating their excellent catalytic performance toward H_2O_2. Similarly, TMB was also

https://doi.org/10.1021/acsomega.4c03460
ACS Omega 2025, 10, 6359−6367

Table 1. Comparison of K_m and V_{max} Value of Au NPs and Other Enzymes

Enzyme	K_m, H_2O_2 (mM)	$V_{max} \times 10^{-8}$ (M S^{-1})	Ref
Au NPs	36.5	47.9	This work
HRP	3.70	8.71	[20]
Fe_3O_4	154	9.78	[20]
AuNPs/NPC	0.38	7.35	[38]
Au/Cu_2O	10.56	6.68	[39]
AuPt/ZIF-8-rGO	0.55	10.9	[40]
Cu_2O/Au−Pt@MOF@F127	22.4	4.05	[41]
Fe_3O_4@SiO_2−NH_2−Au@$Pd_{0.30}$NPs	0.35	6.78	[42]

used as a test substrate to obtain the Michaelis−Menten kinetic curve and Lineweaver−Burk double inverse relationship (Figure S2). The K_m value was found to be 0.142 mM, which was much lower than that of H_2O_2, indicating that Au NPs own a higher POD-like affinity toward TMB substrate than H_2O_2. Besides, the specific activity of Au nanozyme was measured to be 2.78 U mg^{-1} in our revised manuscript, which is comparable to common reported nanozymes (Table S1). Therefore, because of low cost, easy synthesis, and highly comparable catalytic activity, Au NPs is a quite promising POD-like nanozyme for biosensing application.

As known, the POD-like activity of nanozyme and the TMB chromogenic reaction are easily affected by temperature and pH of the reaction solutions.[43] Hence, the influence of temperature and pH on the chromogenic system was studied to better understand the chromogenic performance of the Au nanozyme. As shown in Figure 4a, the chromogenic signal of Au NPs-catalyzed system was enhanced with increasing temperature. When the temperature exceeded 40 °C, the relative signal of oxTMB decreased, which was similar to the temperature limitation of natural enzymes. However, compared with the natural enzyme, the Au nanozymes had higher thermal stability with little change in the relative colorimetric signal over the same temperature range. Figure 4b shows that the relative activity of the Au NPs-catalyzed chromogenic system is more susceptible to pH change. The catalytic performance of Au NPs remained mostly in the pH range from 4.0 to 6.0. When the pH value was less than 3.0 or higher than 7.0, the colorimetric signal was significantly decreased. In addition, the long-term storage study further demonstrated that there was nearly no significant activity loss after 14 days at room temperature, proving their robust stability for further detection (Figure 4c).

3.3. Antioxidant Discrimination by Sensing Array. On the basis of the different POD-like activities of Au NPs under different pH conditions, here, a novel colorimetric sensing array based on Au nanozymes was constructed for identification of biological antioxidants. As shown in Figure 5a, the antioxidants can act on the POD-like Au nanozyme-mediated catalytic system so that the color development of TMB receives different levels of inhibition and "turn-off" signals are generated. As is known, the redox reaction of TMB with H_2O_2 in the presence of POD is a reversible reaction. H_2O_2 is catalyzed by the POD-like nanozyme to generate •OH, and the subsequently oxidized TMB forms an unstable divalent cation radical intermediate, which further forms oxTMB.[37,44] In the presence of an antioxidant, the reaction can proceed in the opposite direction, returning from the oxidized state of TMB to the reduced state of TMB, thus decreasing the colorimetric signal. To prove this, we first use the EPR technique to characterize the change for the production of •OH after typical antioxidant (AA). As shown in Figure 5b, in the presence of AA, the production of •OH is reduced.

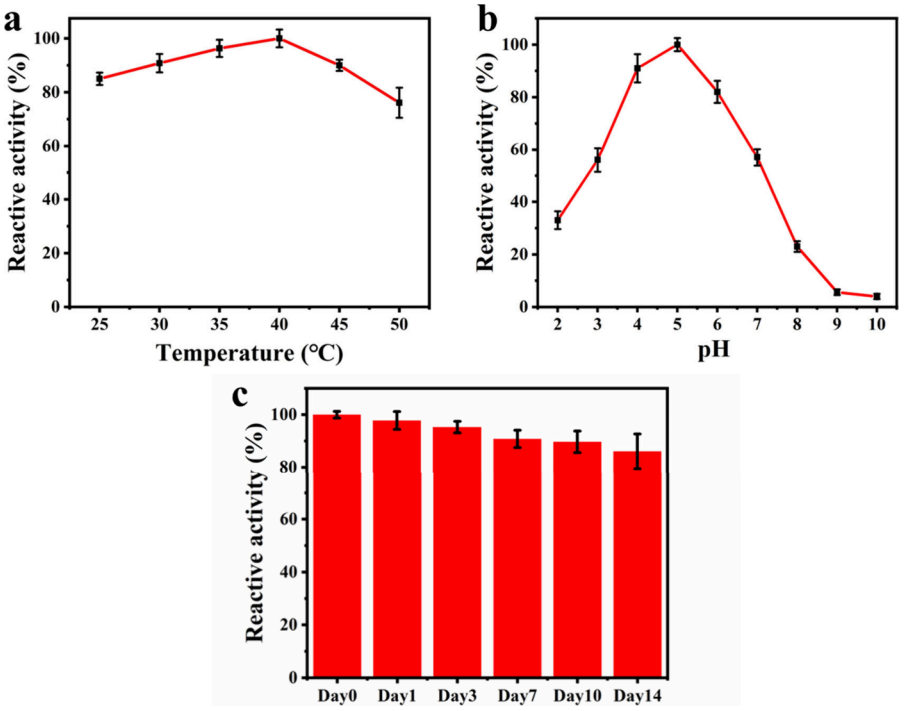

Figure 4. Optimal temperature (a) and pH values (b) for the catalytic chromogenic system of Au NPs. (c) Stability study on catalytic activity of Au nanozyme over 14 days.

https://doi.org/10.1021/acsomega.4c03460
ACS Omega 2025, 10, 6359−6367

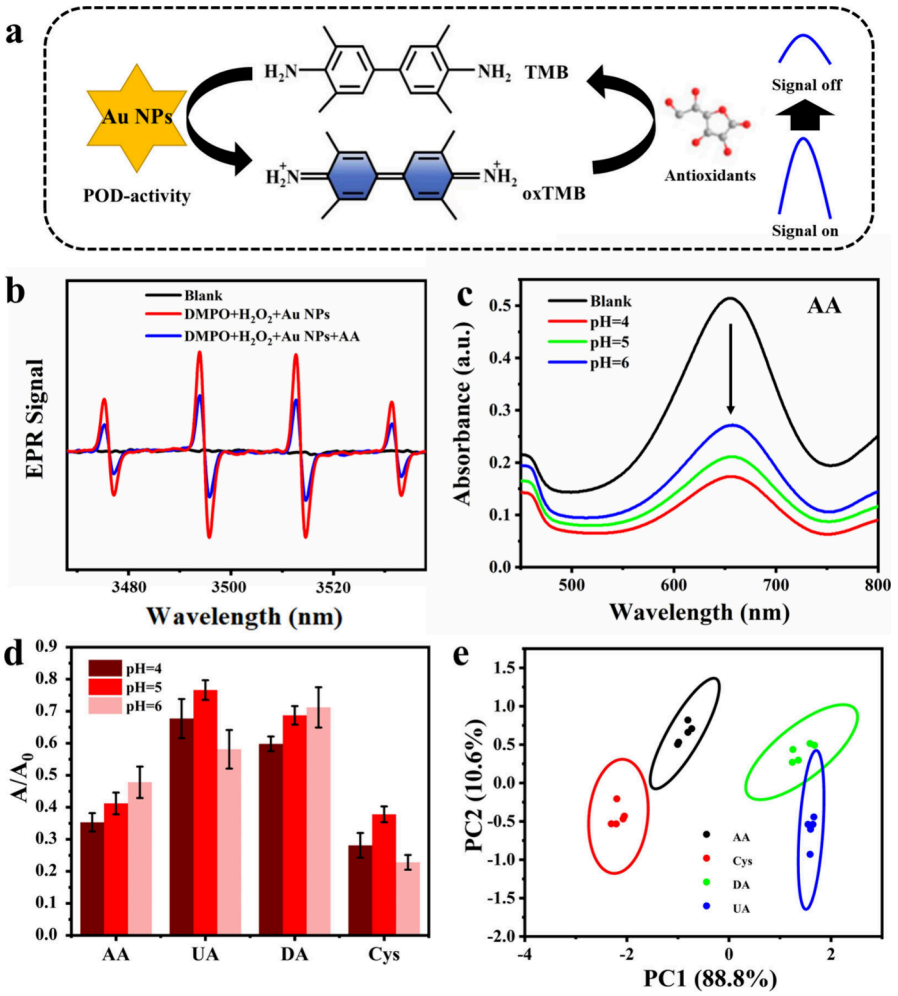

Figure 5. (a) Schematic for reaction process of H_2O_2+TMB+antioxidants system catalyzed using the Au NPs. (b) EPR spectra for the mixture of H_2O_2+DMPO+Au NPs in the absence or presence of AA (1 μM). (c) UV−vis absorption spectra of H_2O_2+TMB+AA system under different pH solutions after reaction for 10 min. (d) Absorbance response patterns (A/A_0) of the Au NPs-based colorimetric sensing array for four antioxidants including AA, UA, DA and Cys. The final concentration of these antioxidants was 1 μM. (e) Two-dimensional PCA canonical score-plot for four-antioxidant discrimination.

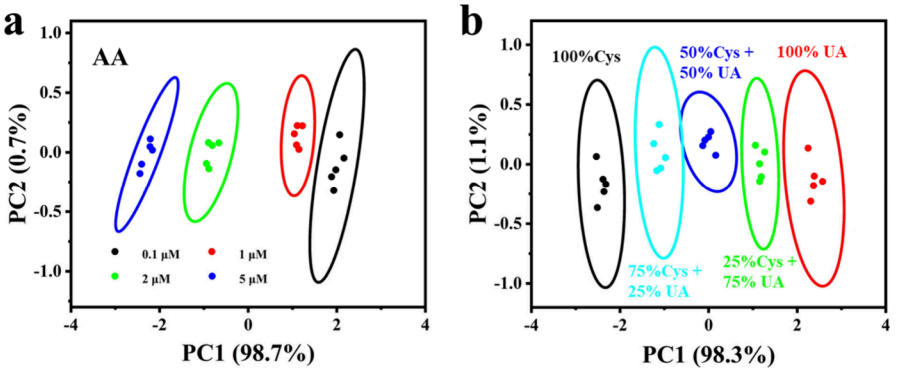

Figure 6. (a) Two-dimensional PCA canonical score-plot for the discrimination of AA at various concentrations. (b) Two-dimensional PCA canonical score-plot for the discrimination of antioxidant mixtures (Cys + UA) with different ratios (total concentration: 10 μM).

Moreover, the signal change of the colorimetric system is quite sensitive at different pH values (Figure 4b). To prove this, the UV−vis spectra of the H_2O_2+TMB+AA system under different pH solutions were recorded and the results show that the signals of the H_2O_2-TMB chromogenic system and the inhibition ability of the various antioxidants on the chromogenic system are significantly different, thus generating differential signals (Figure 5c). We speculate that this mechanism can be used for constructing a novel sensor array. Specifically, the three different pH conditions of the reaction system (pH 4, 5 and 6) led to various POD-like activity of Au NPs and diverse reduction degrees between oxTMB and four types of antioxidants (AA, Cys, DA, and UA). Therefore, the absorbance changes at 652 nm (A/A_0) of each

https://doi.org/10.1021/acsomega.4c03460
ACS Omega 2025, 10, 6359−6367

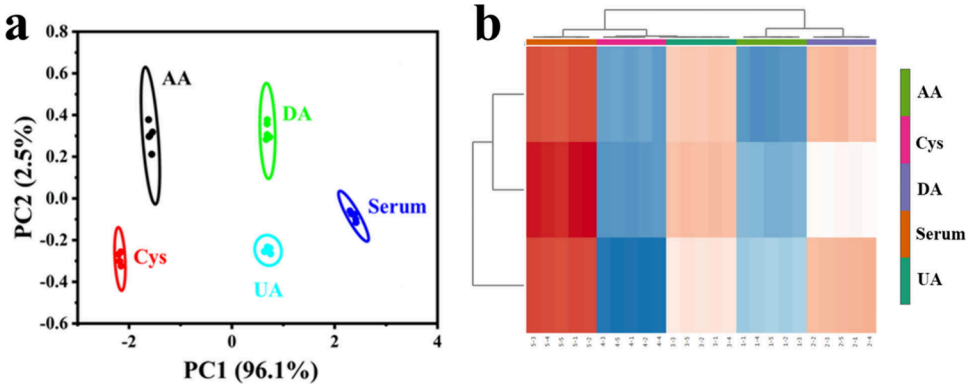

Figure 7. Two-dimension PCA canonical score-plot (a) and HCA heat map (b) for the developed sensing array discriminating Cys, AA, DA, and AA spiked in human serum.

sensing units could be employed as the response patterns for different antioxidant colorimetric discrimination (Figure 5d). A_0 and A stands for the absorbance at 652 nm of Au NPs catalyzed H_2O_2-TMB system in the presence and absence of antioxidants, respectively. As shown in Figure S3, other substances commonly found in serum at the same concentration (1 μM) have no significant effect on the sensor signal, demonstrating the excellent anti-interference ability for practical application. Following this, these colorimetric signals were analyzed by PCA to obtain two-dimensional (2D) typical score plots. As indicated in Figure 5e, the four antioxidants were well-separated from each other and clustered into four groups by the developed sensing array, demonstrating the approach feasibility for the discrimination of antioxidants.

Next, to further verify the quantification and identification capacity of the sensing array, the response signals of analytes with different concentrations (0.1−5 μM) were measured by using AA as a model analyst. As indicated in Figure 6a, the sensing array successfully discriminated the four concentrations of the same target AA, confirming that the nanozyme sensing array possesses distinguishing ability for the individual antioxidant. As shown in Figure S4, the standard curves of AA, Cys, DA, and UA we obtained by plotting the relationship between the concentration of four antioxidants and score of PC. As a result, the linear detection range were 0.1−10 μM and the detection limit of AA, Cys, UA, and DA calculated by the conventional 3σ method was 0.074 μM, 0.062 μM, 0.087 μM, and 0.128 μM, respectively. Figure 6b shows the responses of two mixed antioxidants with different molar ratios. Figure S5 showed that the responses of two different antioxidants with the same mixed ratios. As revealed, the developed sensing array also possessed good distinguishing ability for the mixture of antioxidants. These results further indicate the feasibility of the Au nanozyme-based colorimetric sensing array for simple, rapid, and low-cost colorimetric identification of antioxidants.

3.4. Real Sample Analysis. Subsequently, the practical feasibility of the sensing array to identify antioxidants in biological samples was further verified by adding 1 μM Cys, DA, UA, and AA to a 100-fold diluted human serum sample. As indicated in Figure 7a, the serum real sample produces a certain response due to the presence of certain antioxidants. However, this response does not influence the responses of Cys, DA, UA, and AA, which indicates that the sensing array is resistant to interference in the detection for serum. Furthermore, the four antioxidants were well distinguished from each other by the PCA algorithm, suggesting good potential for practical use of the colorimetric sensing array in complex biological matrices. The heatmap in Figure 7b is obtained by performing HCA clustering analysis on the resulting data. HCA is able to cluster samples with similar response patterns together to achieve an effective classification of the samples, visually identifying similarities and differences between different samples in the sensor array. The color-coded heatmap provides a visual representation of the similarity or distance between data points, making the clustering results of the data more intuitive and understandable. In addition, the HCA cluster analysis heatmap can be used as a tool to validate the results of PCA. By comparing the results of HCA and PCA, the clustering trends and patterns of the data can be further confirmed. Consistent with the findings, the HCA results using the minimum variance (Ward's) method for these five groups are displayed using heat maps, further indicating the accurate distinguished capacity of various serum samples.

4. CONCLUSIONS

In this work, a novel colorimetric sensing array was successfully developed for antioxidant screening and identification based on the POD-like enzyme properties of Au NPs. The Au NPs exhibited excellent nanozymes activity for oxidation of TMB in the presence of H_2O_2, and the different sensor units were achieved by simple adjustments of the three pH values of the chromogenic system. In contrast to single-target sensors with limited specificity, the sensing array successfully discriminates the four antioxidants with the help of two-dimensional PCA of the response. Besides, the sensing array could discriminate different antioxidant mixtures and concentrations. Furthermore, the developed sensing array was also applied for colorimetric identification of multiple antioxidants in real human serum samples. In comparison with common sensing arrays, these single Au nanozyme-based colorimetric sensing arrays have the advantages of low loss, quick response, and simple fabrication. However, in clinical or field settings, the developed sensing arrays may also have some limitations. First, possible variations in the synthesis and surface modification processes of nanomaterials can lead to batch-to-batch variations in the performance of the sensors, affecting their consistency. In addition, practical factors such as temperature, humidity, and light may affect the stability of the optical performance and color change. At the same time, sensor arrays should be carefully considered to avoid material interference in more complex samples and some potential errors caused by

https://doi.org/10.1021/acsomega.4c03460
ACS Omega 2025, 10, 6359−6367

human manipulation. In addition, the proposed sensing array can be further integrated with portable test strips, hand-held devices, and digital software for improving convenience, accuracy, and practicability. However, integrating nanomaterial-based colorimetric sensors with electronic circuits and data processing units into a small device faces technical and engineering challenges. In the future, more varieties of antioxidants and practical biological samples should be studied to validate the robustness of the sensing array for real-world application. We believe that this sensing array can be further extended to the detection of biomolecules related to living systems, which has great potential for biomedical applications.

■ ASSOCIATED CONTENT

Supporting Information

The Supporting Information is available free of charge at https://pubs.acs.org/doi/10.1021/acsomega.4c03460.

Experimental section, time-dependent curves of absorbance at 652 nm, steady-state kinetic test, anti-interference ability test, linear relationship, PCA plot for the discrimination of antioxidant mixtures (PDF)

■ AUTHOR INFORMATION

Corresponding Authors

Yi Lu − *Department of Hepatobiliary & Pancreatic Surgery and Minimally Invasive Surgery, Zhejiang Provincial People's Hospital, Affiliated People's Hospital, Hangzhou Medical College, Hangzhou 311399, China*; Email: lyysz@zju.edu.cn

Xin Zhang − *Department of Pathology, Zhejiang Provincial People's Hospital (Affiliated People's Hospital, Hangzhou Medical College), Hangzhou 311399, China*; Email: zhangxin120189@163.com

Authors

Yu Wang − *Department of Colorectal Surgery, Ningbo Medical Center Li Huili Hospital (Li Huili Hospital affiliated to Ningbo University), Ningbo 315000, China*; orcid.org/0009-0001-1437-018X

Yumeng Liu − *School of Public Health, Hangzhou Medical College, Hangzhou 311399, China*

Lidong Cao − *Department of Hepatobiliary & Pancreatic Surgery and Minimally Invasive Surgery, Zhejiang Provincial People's Hospital, Affiliated People's Hospital, Hangzhou Medical College, Hangzhou 311399, China*

Zunqiang Xiao − *Department of Hepatobiliary & Pancreatic Surgery and Minimally Invasive Surgery, Zhejiang Provincial People's Hospital, Affiliated People's Hospital, Hangzhou Medical College, Hangzhou 311399, China*

Complete contact information is available at: https://pubs.acs.org/10.1021/acsomega.4c03460

Author Contributions

All authors contributed to the study conception and design. Yu Wang conducted methodology, investigation, formal analysis and original draft preparation. Yumeng Liu conducted investigation, validation, data curation, and original draft preparation. Lidong Cao performed validation, data curation, original draft preparation. Zunqiang Xiao performed formal analysis, software, and data curation. Yi Lu performed conceptualization, methodology, review and editing of the manuscript, and funding acquisition. Xin Zhang carried out conceptualization, methodology, formal analysis, review and editing of the manuscript, project administration, and funding acquisition. All authors have read and agreed to the published version of the manuscript.

Notes

The authors declare no competing financial interest.

■ ACKNOWLEDGMENTS

This research was supported by Natural Science Foundation of Ningbo (2023J220), the Zhejiang Provincial Medical and Health Science and Technology Project (2025KY1271), and the Project of Ningbo Leading Medical & Health Discipline(2022-F01).

■ REFERENCES

(1) Halliwell, B.; Zentella, A.; Gomez, E. O.; Kershenobich, D. Antioxidants and human disease: a general introduction. *Nutrition reviews* **1997**, *55* (1), S44.

(2) Albarracin, S. L.; Stab, B.; Casas, Z.; Sutachan, J. J.; Samudio, I.; Gonzalez, J.; Gonzalo, L.; Capani, F.; Morales, L.; Barreto, G. E. Effects of natural antioxidants in neurodegenerative disease. *Nutritional neuroscience* **2012**, *15* (1), 1−9.

(3) Amato, A.; Terzo, S.; Mulè, F. Natural compounds as beneficial antioxidant agents in neurodegenerative disorders: A focus on Alzheimer's disease. *Antioxidants* **2019**, *8* (12), 608.

(4) Dastmalchi, N.; Baradaran, B.; Latifi-Navid, S.; Safaralizadeh, R.; Khojasteh, S. M. B.; Amini, M.; Roshani, E.; Lotfinejad, P. Antioxidants with two faces toward cancer. *Life Sciences* **2020**, *258*, 118186.

(5) Stewart, A. J.; Mullen, W.; Crozier, A. On-line high-performance liquid chromatography analysis of the antioxidant activity of phenolic compounds in green and black tea. *Molecular Nutrition & Food Research* **2005**, *49* (1), 52−60.

(6) Winston, G. W.; Regoli, F.; Dugas, A. J., Jr; Fong, J. H.; Blanchard, K. A. A rapid gas chromatographic assay for determining oxyradical scavenging capacity of antioxidants and biological fluids. *Free Radical Biol. Med.* **1998**, *24* (3), 480−493.

(7) Zheng, Y.; Karimi-Maleh, H.; Fu, L. Evaluation of antioxidants using electrochemical sensors: a bibliometric analysis. *Sensors* **2022**, *22* (9), 3238.

(8) Ghiselli, A.; Serafini, M.; Maiani, G.; Azzini, E.; Ferro-Luzzi, A. A fluorescence-based method for measuring total plasma antioxidant capability. *Free Radical Biol. Med.* **1995**, *18* (1), 29−36.

(9) Zhu, X.; Tang, J.; Ouyang, X.; Liao, Y.; Feng, H.; Yu, J.; Chen, L.; Lu, Y.; Yi, Y.; Tang, L. Multifunctional MnCo@ C yolk-shell nanozymes with smartphone platform for rapid colorimetric analysis of total antioxidant capacity and phenolic compounds. *Biosens. Bioelectron.* **2022**, *216*, 114652.

(10) Zhu, X.; Tang, J.; Ouyang, X.; Liao, Y.; Feng, H.; Yu, J.; Chen, L.; Lu, Y.; Yi, Y.; Tang, L. Hollow NiCo@ C nanozyme-embedded paper-based colorimetric aptasensor for highly sensitive antibiotic detection on a smartphone platform. *Anal. Chem.* **2022**, *94* (48), 16768−16777.

(11) Zhu, X.; Tang, J.; Ouyang, X.; Liao, Y.; Feng, H.; Yu, J.; Chen, L.; Lu, Y.; Yi, Y.; Tang, L. A versatile CuCo@ PDA nanozyme-based aptamer-mediated lateral flow assay for highly sensitive, on-site and dual-readout detection of Aflatoxin B1. *Journal of Hazardous Materials* **2024**, *465*, 133178.

(12) Karadag, A.; Ozcelik, B.; Saner, S. Review of methods to determine antioxidant capacities. *Food analytical methods* **2009**, *2*, 41−60.

(13) Sun, J.; Lu, Y.; He, L.; Pang, J.; Yang, F.; Liu, Y. Colorimetric sensor array based on gold nanoparticles: Design principles and recent advances. *TrAC Trends in Analytical Chemistry* **2020**, *122*, 115754.

(14) Albert, K. J.; Lewis, N. S.; Schauer, C. L.; Sotzing, G. A.; Stitzel, S. E.; Vaid, T. P.; Walt, D. R. Cross-reactive chemical sensor arrays. *Chem. Rev.* **2000**, *100* (7), 2595−2626.

(15) Li, S.; Zhang, Y.; Wang, Q.; Lin, A.; Wei, H. Nanozyme-enabled analytical chemistry. *Anal. Chem.* **2022**, *94* (1), 312−323.
(16) Wang, H.; Wan, K.; Shi, X. Recent advances in nanozyme research. *Advanced materials* **2019**, *31* (45), 1805368.
(17) Liu, W.; Chu, L.; Zhang, C.; Ni, P.; Jiang, Y.; Wang, B.; Lu, Y.; Chen, C. Hemin-assisted synthesis of peroxidase-like Fe-NC nanozymes for detection of ascorbic acid-generating bio-enzymes. *Chemical Engineering Journal* **2021**, *415*, 128876.
(18) Zhang, C.; Chen, C.; Zhao, D.; Kang, G.; Liu, F.; Yang, F.; Lu, Y.; Sun, J. Multienzyme cascades based on highly efficient metal-nitrogen-carbon nanozymes for construction of versatile bioassays. *Anal. Chem.* **2022**, *94* (8), 3485−3493.
(19) Li, Z.; Liu, F.; Chen, C.; Jiang, Y.; Ni, P.; Song, N.; Hu, Y.; Xi, S.; Liang, M.; Lu, Y. Regulating the N coordination environment of Co single-atom nanozymes for highly efficient oxidase mimics. *Nano Lett.* **2023**, *23* (4), 1505−1513.
(20) Gao, L.; Zhuang, J.; Nie, L.; Zhang, J.; Zhang, Y.; Gu, N.; Wang, T.; Feng, J.; Yang, D.; Perrett, S.; Yan, X. Intrinsic peroxidase-like activity of ferromagnetic nanoparticles. *Nature Nanotechnol.* **2007**, *2* (9), 577−583.
(21) Lou-Franco, J.; Das, B.; Elliott, C.; Cao, C. Gold nanozymes: from concept to biomedical applications. *Nano-Micro Letters* **2021**, *13*, 1−36.
(22) Zhang, D.-Y.; Liu, H.; Younis, M. R.; Lei, S.; Yang, C.; Lin, J.; Qu, J.; Huang, P. Ultrasmall platinum nanozymes as broad-spectrum antioxidants for theranostic application in acute kidney injury. *Chemical Engineering Journal* **2021**, *409*, 127371.
(23) Huo, J.; Hao, J.; Mu, J.; Wang, Y. Surface modification of Co3O4 nanoplates as efficient peroxidase nanozymes for biosensing application. *ACS Applied Bio Materials* **2021**, *4* (4), 3443−3452.
(24) Wu, J.; Yang, Q.; Li, Q.; Li, H.; Li, F. Two-dimensional MnO2 nanozyme-mediated homogeneous electrochemical detection of organophosphate pesticides without the interference of H2O2 and color. *Anal. Chem.* **2021**, *93* (8), 4084−4091.
(25) Chen, J.; Xu, F.; Zhang, Q.; Li, S. N-doped MoS2-nanoflowers as peroxidase-like nanozymes for total antioxidant capacity assay. *Anal. Chim. Acta* **2021**, *1180*, 338740.
(26) Li, X.; Kong, C.; Chen, Z. Colorimetric sensor arrays for antioxidant discrimination based on the inhibition of the oxidation reaction between 3, 3′, 5, 5′-tetramethylbenzidine and hydrogen peroxides. *ACS Appl. Mater. Interfaces* **2019**, *11* (9), 9504−9509.
(27) Jing, W.; Cui, X.; Kong, F.; Wei, W.; Li, Y.; Fan, L.; Li, X. Fe-N/C single-atom nanozyme-based colorimetric sensor array for discriminating multiple biological antioxidants. *Analyst* **2021**, *146* (1), 207−212.
(28) Jans, H.; Huo, Q. Gold nanoparticle-enabled biological and chemical detection and analysis. *Chem. Soc. Rev.* **2012**, *41* (7), 2849−2866.
(29) Lopes, G.; Cennamo, N.; Zeni, L.; Singh, R.; Kumar, S.; Fernandes, A. J.; Costa, F.; Pereira, S. O.; Marques, C. Innovative optical pH sensors for the aquaculture sector: Comprehensive characterization of a cost-effective solution. *Optics & Laser Technology* **2024**, *171*, 110355.
(30) Singh, R.; Zhang, W.; Liu, X.; Zhang, B.; Kumar, S. WaveFlex Biosensor: MXene-Immobilized W-shaped Fiber-Based LSPR sensor for highly selective tyramine detection. *Optics & Laser Technology* **2024**, *171*, 110357.
(31) Gomes, H. C.; Liu, X.; Fernandes, A.; Moreirinha, C.; Singh, R.; Kumar, S.; Costa, F.; Santos, N.; Marques, C. Laser-Induced graphene-based Fabry-Pérot cavity label-free immunosensors for the quantification of cortisol. *Sensors and Actuators Reports* **2024**, *7*, 100186.
(32) Xu, J. X.; Alom, M. S.; Yadav, R.; Fitzkee, N. C. Predicting protein function and orientation on a gold nanoparticle surface using a residue-based affinity scale. *Nat. Commun.* **2022**, *13* (1), 7313.
(33) Hafez, M. E.; Ma, H.; Ma, W.; Long, Y. T. Unveiling the intrinsic catalytic activities of single-gold-nanoparticle-based enzyme mimetics. *Angew. Chem.* **2019**, *131* (19), 6393−6398.
(34) Kim, H.; Park, M.; Hwang, J.; Kim, J. H.; Chung, D.-R.; Lee, K.-s.; Kang, M. Development of label-free colorimetric assay for MERS-CoV using gold nanoparticles. *ACS sensors* **2019**, *4* (5), 1306−1312.
(35) Shen, L.; Khan, M. A.; Wu, X.; Cai, J.; Lu, T.; Ning, T.; Liu, Z.; Lu, W.; Ye, D.; Zhao, H.; Zhang, J. Fe-N-C single-atom nanozymes based sensor array for dual signal selective determination of antioxidants. *Biosens. Bioelectron.* **2022**, *205*, 114097.
(36) Nontawong, N.; Ngaosri, P.; Chunta, S.; Jarujamrus, P.; Nacapricha, D.; Lieberzeit, P. A.; Amatatongchai, M. Smart sensor for assessment of oxidative/nitrative stress biomarkers using a dual-imprinted electrochemical paper-based analytical device. *Anal. Chim. Acta* **2022**, *1191*, 339363.
(37) Zhou, X.; Shao, Z.; Yan, S.; Lin, Y.; Liu, Y.; Feng, X.; Sha, J.; Ding, L.; Wang, K. Coencapsulating TMB Probes and Bimetallic MOF Nanozymes in a Hydrogel Patch for Fabricating Reusable Visual VC Sensors. *Anal. Chem.* **2024**, *96* (43), 17310−17318.
(38) Chen, Z.; Zhang, T.; Liu, Y.; Zhang, X.; Chen, L.; Zhang, Z.; Lu, N. Nanozyme Sensor Based on Au Nanoparticles/N-Doped Porous Carbon Composites for Biosensing. *ACS Applied Nano Materials* **2024**, *7*, 3645.
(39) Jiao, A.; Xu, L.; Tian, Y.; Cui, Q.; Liu, X.; Chen, M. Cu2O nanocubes-grafted highly dense Au nanoparticles with modulated electronic structures for improving peroxidase catalytic performances. *Talanta* **2021**, *225*, 121990.
(40) Zhang, T.; Xing, Y.; Song, Y.; Gu, Y.; Yan, X.; Lu, N.; Liu, H.; Xu, Z.; Xu, H.; Zhang, Z.; Yang, M. Aupt/mof-graphene: a synergistic catalyst with surprisingly high peroxidase-like activity and its application for H2O2 detection. *Analytical chemistry* **2019**, *91* (16), 10589−10595.
(41) Cheng, Y.; Xia, Y. D.; Sun, Y. Q.; Wang, Y.; Yin, X. B. Three-in-One" Nanozyme Composite for Augmented Cascade Catalytic Tumor Therapy. *Adv. Mater.* **2024**, *36*, 2308033.
(42) Adeniyi, O.; Sicwetsha, S.; Mashazi, P. Nanomagnet-silica nanoparticles decorated with Au@ Pd for enhanced peroxidase-like activity and colorimetric glucose sensing. *ACS Appl. Mater. Interfaces* **2020**, *12* (2), 1973−1987.
(43) Duan, W.; Qiu, Z.; Cao, S.; Guo, Q.; Huang, J.; Xing, J.; Lu, X.; Zeng, J. Pd-Fe3O4 Janus nanozyme with rational design for ultrasensitive colorimetric detection of biothiols. *Biosens. Bioelectron.* **2022**, *196*, 113724.
(44) Zhang, X.; Yang, Q.; Lang, Y.; Jiang, X.; Wu, P. Rationale of 3, 3′, 5, 5′-tetramethylbenzidine as the chromogenic substrate in colorimetric analysis. *Anal. Chem.* **2020**, *92* (18), 12400−12406.

https://doi.org/10.1021/acsomega.4c03460
ACS Omega 2025, 10, 6359−6367